Journal of The Electrochemical Society, **158** (4) G97-G102 (2011)
0013-4651/2011/158(4)/G97/6/$28.00 © The Electrochemical Society

In Situ Two-Step Plasma Enhanced Atomic Layer Deposition of Ru/RuN_x Barriers for Seedless Copper Electroplating

Chih-Chieh Chang and Fu-Ming Pan[z]

Department of Materials Science and Engineering, National Chiao-Tung University, Hsinchu, Taiwan 30050

The study prepared Ru/RuN_x bilayer barriers on mesoporous SiO_2 (*mp*-SiO_2) dielectric layers for direct Cu electroplating applications using in situ two-step plasma-enhanced atomic chemical vapor deposition (PEALD). For the 5 nm thick Ru/RuN_x bilayer deposited at 200°C, obvious thermal decomposition begins at temperatures lower than 400°C. Copper can be successfully electroplated on the as-deposited Ru/RuN_x bilayer, and the Cu/Ru/RuN_x/*mp*-SiO_2 film stack can withstand thermal treatment at temperatures up to 500°C without significant physical and chemical degradations according to TEM and SIMS analyses. The study shows that the electroplated Cu layer behaves like a passivation layer that improves the thermal stability of the Ru/RuN_x barrier during the thermal annealing. Pull-off tensile test shows that interfaces in the Cu/Ru/RuN_x/*mp*-SiO_2 film stack have good adhesion strength, but delamination occurs at the interface between the Ru/RuN_x bilayer and the *mp*-SiO_2 layer at 600°C, resulting in Cu and Ru diffusion into the dielectric layer. The study has demonstrated that the PEALD Ru/RuN_x bilayer structure prepared using the in situ two-step approach is suitable for the seedless Cu electroplating process in nanometer scale interconnect technology.
© 2011 The Electrochemical Society. [DOI: 10.1149/1.3554734] All rights reserved.

Manuscript submitted October 18, 2010; revised manuscript received December 30, 2010. Published March 2, 2011.

Traditional Cu interconnect technology requires a Cu seed layer grown on the diffusion barrier for the Cu electroplating process. A seed/glue/barrier tri-layer structure, such as the Cu seed/Ta/TaN film stack, is generally used in the dual-damascene process for better adhesion and microstructure. Physical vapor deposition (PVD) is the most widely used method to deposit the Cu seed layer and the barrier layer. However, the PVD approach may present scaling difficulties for sub-32 nm technology nodes because of intrinsic drawbacks of the PVD process, such as poor conformality and thickness uniformity in nanometer scale. To avoid these intrinsic shortcomings associated with the PVD process, atomic layer chemical vapor deposition (ALD) has long been regarded as a promising alternative to the PVD process for the dual-damascene technology. The feature of self-limiting surface reactions in the ALD process provides accurate thickness control in the atomic scale as well as excellent conformity and uniformity for patterns with a high aspect ratio over a large area.

Because a diffusion barrier with a thickness <5 nm is required for sub-32 nm technology nodes,[1] various diffusion barriers deposited by ALD have been studied in the past decade.[2–4] Besides, PVD-deposited Cu seed layers have a minimum thickness limit of ~30–40 nm, and are, therefore, inappropriate for the Cu dual-damascene technique for sub-32 nm nodes because of the poor confomality inherent to PVD.[5] Much effort has been done in order to replace the Cu PVD seed layer with materials that can be properly processed in the dual-damascene technique for future technology nodes. Some Cu-plateable metals, such as Ru, Ir, and Os,[6–8] have attracted considerable attention because they also have good barrier properties for copper. Among various candidate metals, Ru receives the most study because of its low electrical resistivity and negligible solubility in copper at 900°C.[9] Ru is also a stable transition metal in air and has good wettability with Cu. However, polycrystalline Ru is unsuitable for serving as a Cu diffusion barrier because its columnar grain structure provides a fast diffusion path for Cu atoms at 450°C.[10] On the other hand, amorphous Ru demonstrates better diffusion barrier properties than the polycrystalline Ru barrier, and has a higher adhesion strength with Cu.[11] When a high level of nitrogen atoms is dissolved in an Ru film, the nitrided Ru film usually has a nanocrystalline structure with a very short range ordering,[12] or even exhibits an amorphous form. Several recent studies demonstrated that nitrided Ru barriers prepared by PVD had satisfactory barrier characteristics.[11–14] However, RuN_x has a relatively high electrical resistance, making direct Cu electrodeposition difficult on the RuN_x surface. In this study, we deposited Ru/RuN_x bilayer barriers on mesoporous SiO_2 (thereafter denoted by *mp*-SiO_2) dielectric layers by an in situ two-step plasma-enhanced ALD (PEALD) process, and copper could be directly electrodeposited on the as-deposited Ru/RuN_x barrier. The as-deposited Ru/RuN_x bilayer is thermally degraded at temperatures below 300°C as a result of decomposition of the RuN_x layer. However, if thermal annealing is carried out after the Ru/RuN_x bilayer is electroplated by a Cu layer, the RuN_x decomposition is suppressed, and the Cu/Ru/RuNx/*mp*-SiO_2 multilayer stack can withstand thermal treatment at temperatures up to 500°C without significant degradation in mechanical and electrical properties.

Experimental

PEALD RuN_x thin films were deposited on plasma-treated *mp*-SiO_2 thin films, which were spin-coated on 6-in. p-type Si wafers, at 200°C using bis(ethylcyclopentadienyl)ruthenium [$Ru(EtCp)_2$] and a gas mixture of H_2/N_2 as the Ru precursor and the reducing reactant, respectively. The preparation of the *mp*-SiO_2 thin film and the pore sealing of the porous dielectric by oxygen plasma treatment have been described previously.[15,16] The PEALD system had a base pressure of 5×10^{-4} Torr. One cycle of the PEALD RuN_x deposition process consisted of four consecutive gas pulses, including the $Ru(EtCp)_2$ precursor injection pulse, the Ar purge pulse with a flow rate of 50 sccm, the H_2/N_2 plasma nitridation pulse, and another Ar purge pulse. During the PEALD RuN_x deposition, the stainless steel tube containing the precursor was maintained at 75°C to produce an adequate amount of vapor, which was carried by argon gas at a flow rate of 50 sccm. The gas line delivering $Ru(EtCp)_2$ was heated at 80°C by heating tapes to prevent the precursor from condensation. For the deposition of metallic Ru thin films, an H_2 gas pulse was used instead of the H_2/N_2 pulse. Cu electroplating was carried out at room temperature using a custom plating system with an electrolyte bath comprised of H_2SO_4, $CuSO_4 \cdot 5H_2O$ and HCl. The study used a current density of 10 mA/cm^2 for the Cu electroplating. Thermal anneal treatment of the samples was carried out in a vaccum funace at 10^{-7} Torr.

The surface morphology of the RuN_x thin film was examined by scanning electron microscopy (SEM, JEOL JSM-6500 F) and atomic force microscopy (AFM, Digital Instruments. NanoScope E). The surface chemical composition was characterized by x-ray photoelectron spectroscopy (XPS, thermo VG 350) using the Mg K_α x-ray radiation. The XPS spectra presented in the report have been calibrated with the binding energy of the Pt $4f_{7/2}$ electron. A grazing incident angle X-ray diffraction (XRD) system (Bede D1) was used to characterize the crystallinity and the chemical phase of the PEALD and the electroplated thin films, using Cu K_α radiation with 2θ ranging from 30 to 60°. The microstructure of the Cu/Ru/RuN_x/*mp*-SiO_2 film stack was studied by transmission electron microscopy

[z] E-mail: fmpan@faculty.nctu.edu.tw

Downloaded on 2014-04-24 to IP 140.113.38.11 address. Redistribution subject to ECS terms of use (see ecsdl.org/site/terms_use) unless CC License in place (see abstract).

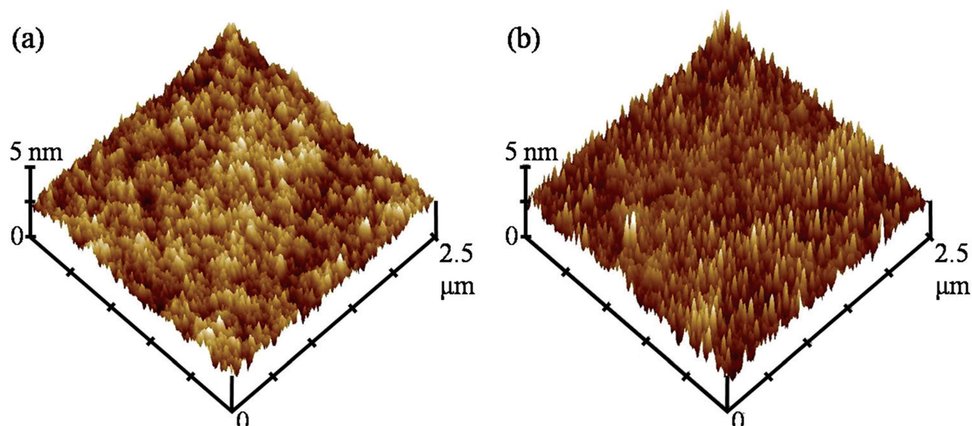

Figure 1. (Color online) AFM images of the mesoporous silica thin film before (a) and after (b) the deposition of the PEALD Ru/RuN_x bilayer of 4 nm in thickness.

(TEM, Philips tacnai 20). Auger electron spectroscopy (AES, thermo VG 350) and secondary ion mass spectroscopy (SIMS, Cameca ION-TOF) were used to examine the elemental distribution in the film stacks.

The adhesion strength of interfaces in the $Cu/Ru/RuN_x/mp\text{-}SiO_2$ film stack was measured by the pull-off tensile test. An Al rod (2.7 mm diameter) was glued onto the Cu surface with epoxy resin and cured at 150°C for 1 h. The rod was pulled at a progressively increasing load of 0–100 kg until delamination occurred to the film stack. Electrical measurement was performed with an HP 4145B semiconductor parameter analyzer using the metal-insulator-semiconductor (MIS) capacitor measurement structure with an Al thin film sputter-deposited on the Si wafer as the backside electrode. The MIS capacitor structure has an area of 0.25π mm^2. The sheet resistance of the electroplated Cu thin film was measured with a four-point probe measurement system (Napson RT-80).

Results and Discussion

The PEALD RuN_x diffusion barrier was deposited at 200°C on the oxygen-plasma treated *mp*-SiO_2 layer of 100 nm in thickness, which had a dense surface oxide layer and showed good dielectric properties as reported previously.[15] The pore sealing treatment can prevent Ru precursor species from penetrating into the porous dielectric layer during the PEALD RuN_x barrier deposition. The growth rate per cycle of the PEALD RuN_x film increases with the $Ru(EtCp)_2$ pulse time and becomes saturated at about 0.038 nm/cycle when the $Ru(EtCp)_2$ pulse time exceeded 5 s. The saturation of the growth per cycle is characteristic for a self-limited reaction.[17] Direct Cu electroplating could not be performed on the 4 nm thick RuN_x thin film because RuN_x has a high electrical resistivity. A previous study showed that a sputter-deposited RuN_x film had a sheet resistance ten times higher than a metallic Ru thin film.[6] To reduce the sheet resistance of the barrier layer, we deposited metallic Ru on the RuN_x thin film using the in situ two-step PEALD process. The preparation of the Ru/RuN_x bilayer used 90 PEALD cycles for the RuN_x bottom layer and ten PEALD cycles for the Ru top layer. The metallic Ru layer was deposited under process conditions like the RuN_x layer except that the H_2/N_2 mixture-gas pulse was replaced with an H_2 gas pulse. The growth rate of the PEALD Ru thin film under the process condition is about 0.03 nm/cycle according to TEM analysis.

Figure 1 shows AFM images of the *mp*-SiO_2 substrate before and after the deposition of the PEALD Ru/RuN_x bilayer. The in situ two-step PEALD process produced a smooth Ru/RuN_x bilayer barrier of good conformality. The root-mean-square (rms) surface roughness of the mesoporous silica substrate and the Ru/RuN_x bilayer is 0.5 and 0.8 nm, respectively. The smooth surface is crucial for a seedless Cu electroplating process, which requires a continuous barrier layer of ultrathin thickness. Ruthenium nitride is thermally unstable at temperatures higher than 275°C, at which it decomposes into metallic Ru and nitrogen.[11] The low decomposition temperature cannot meet the process temperature requirement for the Cu dual-damascene process. To evaluate the thermal stability of the PEALD Ru/RuN_x bilayer on the porous silica dielectric, we annealed the samples at various temperatures in vacuum (10^{-7} Torr) for 30 min, and examined the microstructure and chemical states of the annealed Ru/RuN_x film stack. Figure 2 shows SEM images of the thermally annealed Ru/RuN_x bilayer. When the sample is annealed at 400°C, slight film rupture occurs to the sample surface (see Fig. 2b), indicating thermal decomposition of RuN_x has already led to film degradation. For the sample annealed at 500°C, the SEM image (Fig. 2c) shows that particles, with a size ranging from a few nanometers to one tenth of a micrometer, scatter on the sample surface. The particle growth becomes much more severe for the sample annealed at 600°C as shown by Fig. 2d. XPS and XRD analyses discussed later suggest that these particles are discrete Ru islands.

Figures 3a and 3b show the $Ru(3p_{3/2})$ and N(1s) XPS spectra, respectively, of the Ru/RuN_x bilayer as a function of the annealing temperature. To determine the $Ru(3p_{3/2})$ electron energy for metallic Ru and nitrided Ru, we first performed XPS analysis separately for the as-deposited Ru and the as-deposited RuN_x thin films. The masured $Ru(3p_{3/2})$ energy is 462.0 and 463.0 eV for metallic Ru and nitrided Ru, respectively. Nonlinear least square curve fitting of the $Ru(3p_{3/2})$ peak, assuming a Gaussian peak shape, shows that the

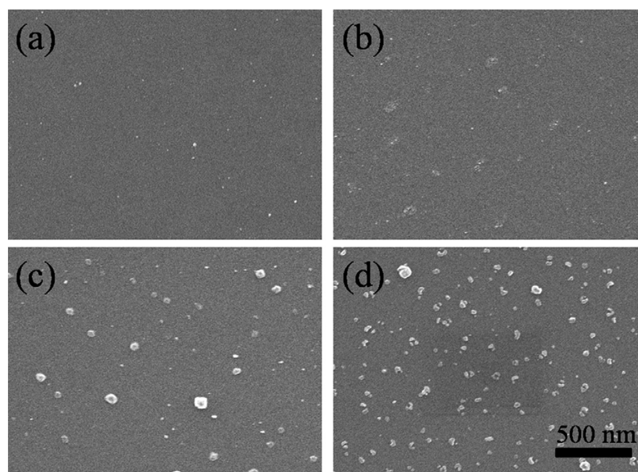

Figure 2. SEM images of (a) the as-deposited, (b) the 400°C-annealed, (c) the 500°C-annealed, and (d) the 600°C-annealed Ru/RuN_x bilayers deposited on the mesoporous silica film.

Downloaded on 2014-04-24 to IP 140.113.38.11 address. Redistribution subject to ECS terms of use (see ecsdl.org/site/terms_use) unless CC License in place (see abstract).

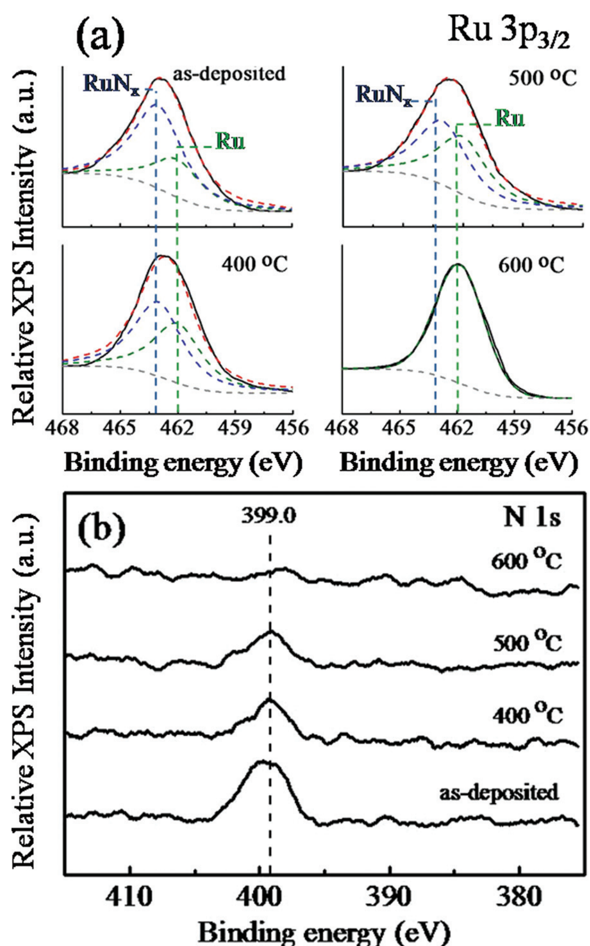

Figure 3. (Color online) (a) $Ru(3p_{3/2})$ and (b) N(1s) XPS spectra of the Ru/RuN_x bilayer sample as a function of the annealing temperature. The two curve-fitted $Ru(3p_{3/2})$ peaks at 462.0 and 463.0 eV represent metallic Ru and nitrided Ru, respectively.

composition of metallic Ru in the bilayer sample increases with the annealing temperature. In contrast, the N(1s) signal decreases with increasing the annealing temperature. Compared with the as-deposited bilayer, the 400°C-annealed bilayer has a larger metallic Ru composition and a smaller N(1s) signal, suggesting thermal decomposition already occurs to the underlying RuN_x layer at 400°C. For the 500°C-annealed bilayer, thermal degradation is more severe as indicated by the larger decrease in the $Ru(3p_{3/2})$ signal ratio of Ru to RuN_x. The XPS result is in agreement with the SEM observation discussed above, which shows the presence of voids and particles on the annealed bilayer. The N(1s) signal of the bilayer annealed at 600°C is barely detected, indicating that RuN_x is likely completely decomposed into metallic Ru phase.

Figure 4a shows XRD spectra of the Ru/RuN_x bilayer annealed at different temperatures. The XRD spectra of the as-deposited and the 400°C-annealed samples show a very broad peak centered at $2\theta = 33.5°$. The broad peak is likely due to the presence of RuN_x nanocrystalline clusters in the amorphous matrix of the Ru/RuN_x bilayer.[11] For the bilayer annealed at 500°C, the XRD spectrum becomes nearly featureless, suggesting that thermal degradation of the Ru/RuN_x bilayer continues to proceed when the annealing temperature is increased. In the XRD spectrum of the bilayer annealed at 600°C, a very weak and broad peak, which is just above the noise level, is situated around 43.1°. The presence of the weak peak can be perceived by comparison, between the as-deposited and the 400°C-annealed samples, of the spectrum profile within the range from 40 to 47°. The peak may result from the overlap of the diffraction peaks due to the (002) (42.15°) and (101) (44.00°) lattice planes of the hexagonal Ru crystal structure.[17,18] Because the 600°C-annealed bilayer comprises only metallic Ru according to the XPS and XRD analyses, particles observed in the SEM image of Fig. 2d are most likely Ru particles.

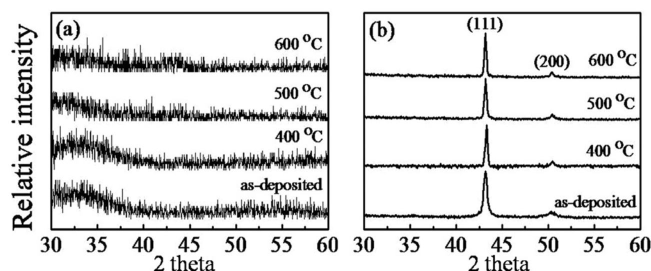

Figure 4. XRD spectra of (a) the Ru/RuN_x bilayer deposited on the *mp*-SiO_2 layer, and (b) the $Cu/Ru/RuN_x$/*mp*-SiO_2 multilayer stacks as a function of the annealing temperature.

The thermal degradation of the RuN_x layer in the bilayer structure has adverse effects on direct Cu electroplating. Under the electroplating condition of the study, Cu could be electrodeposited on the as-deposited Ru/RuN_x bilayer, but Cu electrodeposition on a pure RuN_x layer and the Ru/RuN_x bilayer annealed at 400 and 500°C was unsuccessful. Noted that the 400°C-annealed Ru/RuN_x bilayer still keeps a continuous film surface according to the SEM image in Fig. 2c. The failure in the Cu electroplating indicates that the 400°C-annealed bilayer has a significantly higher electrical resistance than the as-deposited one. It is likely that the partial thermal decomposition of the underlying RuN_x layer at 400°C might drive nitrogen out-diffuse from the underlying RuN_x layer into the upper metallic Ru layer, thereby increasing the sheet resistance of the bilayer structure. To ensure successful Cu electroplating, we performed the thermal treatment only after Cu was electroplated on the as-deposited Ru/RuN_x bilayer. Figure 4b shows XRD spectra of a 100 nm thick Cu film electroplated on the Ru/RuN_x bilayer as a function of the annealing temperature. The Cu(111) and Cu(200) peaks are the only two diffraction peaks detected in the spectra of the annealed samples, and the electroplated Cu has a high degree of the (111) texture. The preferential texture is desirable for Cu interconnects because Cu films with the (111) preferential orientation are four times better in electromigration resistance than those with the (200) orientation.[19] The as-deposited Cu thin film has a sheet resistivity of 21.0 m$\Omega/\square$, and the sheet resistivity of the electroplated Cu layer decreases to 14.1 m$\Omega/\square$ for all the $Cu/Ru/RuN_x$ film stacks annealed at temperatures between 400 and 600°C. The sheet resistivity of a thin film is an indirect indication of the crystallinity and the chemical purity of the thin film. Although, as discussed later, thermal annealing at 600°C leads to chemical and microstructure breakdowns for the $Cu/Ru/RuN_x$ film stack, the breakdowns result in an insignificant change in the sheet resistivity of the film stack, indicating that the barrier failure has little adverse effect on the material properties of the electroplated Cu thin film.

Figure 5 shows cross-sectional SEM images of the $Cu/Ru/RuN_x$/*mp*-SiO_2 multilayer stack, as a function of the annealing temperature. For samples annealed at 500°C and below, the interface between the Ru/RuN_x barrier layer and the Cu layer is free from particles and delamination (Figs. 5a and 5c). On the other hand, localized interface delamination occurs to the sample annealed at 600°C (Fig. 5d). Auger depth profiling and ESCA analyses reveal that the delamination develops at the interface between the Ru/RuN_x barrier layer and the *mp*-SiO_2 layer. Figure 6 shows the Auger depth profile of the 600°C-annealed multilayer sample with the delaminated layer being mecahnically removed. The depth profile clearly indicates that SiO_2 is the matrix and Ru has diffused into the *mp*-SiO_2 layer. Cu is also present on the surface of the separated substrate. The diffusion of Ru and Cu into the mesoporous dielectric layer can be more clearly seen in the SIMS depth profile discussed later.

Downloaded on 2014-04-24 to IP 140.113.38.11 address. Redistribution subject to ECS terms of use (see ecsdl.org/site/terms_use) unless CC License in place (see abstract).

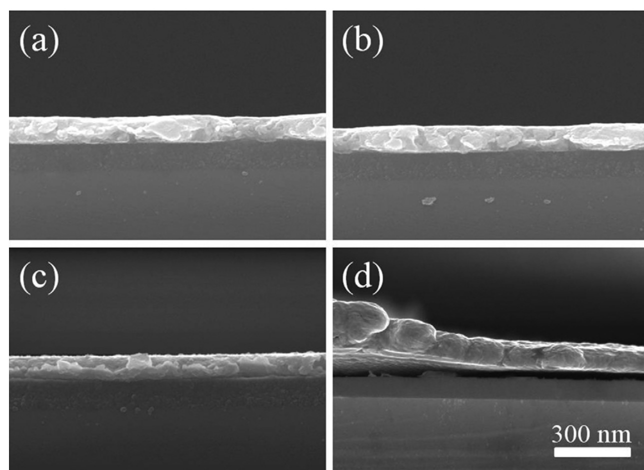

Figure 5. Cross-sectional SEM images of (a) the as-prepared, (b) the 400°C-annealed, (c) the 500°C-annealed, and (d) the 600°C-annealed $Cu/Ru/RuN_x$/*mp*-SiO_2 multilayer stacks.

To furher clarify the integrity of the interfaces in the Cu/Ru/RuN_x/*mp*-SiO_2 mutilayer stack after the thermal anneal, we used TEM to examine the annealed samples. Cross-sectional TEM images of Figs. 7a and 7b clearly show that the interfaces of the Ru/RuN_x barrier with the Cu layer and with the mesoporous SiO_2 substrate are physically intact after the sample is annealed at temperatures below 500°C. The high resolution TEM image in Fig. 7c demonstrates that the Ru/RuN_x layer in the 500°C-annealed sample is amorphous without obvious flaw, and has a uniform thickness close to that of the as-prepared multilayer stack. Unlike the bare Ru/RuN_x layer, the Cu capped barrier bilayer is free from crevice and particle at the interface after the thermal anneal. For the 600°C-annealed $Cu/Ru/RuN_x$/*mp*-SiO_2 mutilayer stack, the TEM image (Fig. 7d) shows the presence of a ~10 nm wide band of darker contrast in the surface region of the *mp*-SiO_2 layer. The dark band is absent in the TEM images of the 400- and the 500°C-annealed samples, and it must result from Ru and Cu diffusion into the *mp*-SiO_2 layer as shown by the Auger depth profile in Fig. 6. SIMS was also used to study if the Ru/RuN_x bilayer was an effective Cu diffusion barrier at temperatures ≤500°C. Figure 8 shows SIMS depth profiles of the thermally annealed $Cu/Ru/RuN_x$/*mp*-SiO_2 mutilayer stack. The 400- and the 500°C-annealed samples show little difference in the depth profile feature for all the analyzed elements. Noted that the Ru and N signals are entirely present in the signal regime of the *mp*-SiO_2 layer, and the Cu signal also extends into the dielectric layer with a

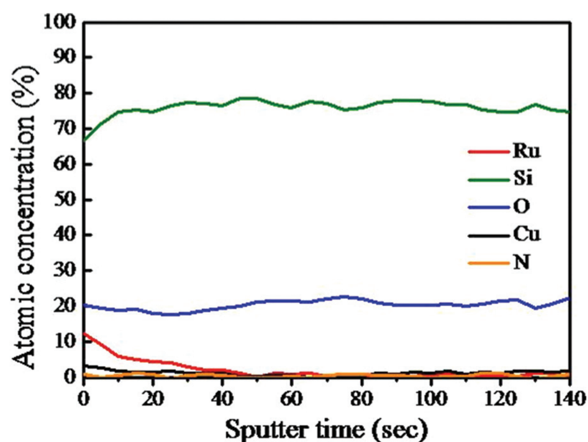

Figure 6. (Color online) Auger depth profiles of the 600°C-annealed Cu/Ru/RuN_x/*mp*-SiO_2 multilayer sample with the delaminated top layer being removed.

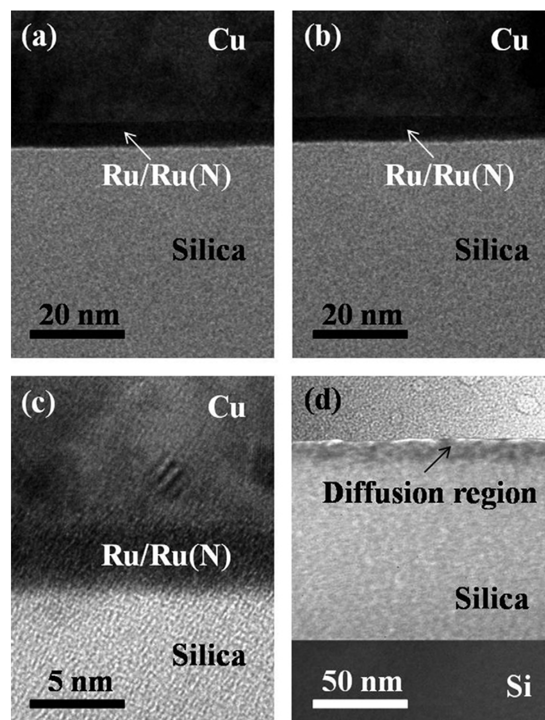

Figure 7. Cross-sectional TEM images of (a) the 400°C-annealed, (b) the 500°C-annealed, (c) the 500°C-annealed (in high resolution), and (d) the 600°C-annealed $Cu/Ru/RuN_x$/*mp*-SiO_2 multilayer stacks. To prepare the TEM specimen for the 600°C-annealed sample, the top delaminated layer was removed from the substrate.

rapid drop at the same depth as the Ru and N signal drops. However, the signal penetration cannot represent the true elemental distribution at the interface of the ultrathin Ru/RuN_x layer with the *mp*-SiO_2 layer, but is likely a result of artifacts of the SIMS analysis, such as ion mixing and Gibbsian segregation.[20] The concurrent and rapid drop for the Cu, Ru and N signals at the interface suggests that the Ru/RuN_x barrier can effectively retard Cu diffusion into the dielectric layer at temperatures as high as 500°C. Combined with the TEM study discussed above, the SIMS analysis suggests that the electrodeposited Cu film behaves like a passivation layer that can effectively impede thermal degradation of the PEALD Ru/RuN_x barrier at 500°C and below. For the multilayer stack annealed at 600°C, the profile shape of the Ru, N and Cu signals is markedly changed and the nitrogen content is greatly reduced, strongly indicating the occurrence of chemical breakdown of the barrier layer. The breakdown results in metal diffusion into the *mp*-SiO_2 layer as revealed by the gradual signal penetration of Ru and Cu as well as the relatively high background of the Cu signal in the SiO_2 region.

We performed leakage current measurements to study the effect of thermal annealing on the electrical properties of the $Cu/Ru/RuN_x$/*mp*-silica multilayer stack. The electroplated copper was used as the top electrode and an Al thin film sputter-deposited on the back side of the Si wafer was the bottom electrode. Figure 9 shows the leakage current density versus the electric field for the annealed multilayer samples. Prior to the thermal treatment, the multilayer sample has a leakage current density of 7.2×10^{-6} A/cm^2 at the stress field of 1 MV/cm. The leakage current density slightly increases to 8.1 $\times 10^{-6}$ A/cm^2 after the sample is annealed at 400°C. For the 500°C-annealed sample, a much larger leakage current density (2.1×10^{-5} A/cm^2) was measured, indicating that the Ru/RuN_x barrier did suffer greater thermal degradation at 500°C than at 400°C. The leakage current density of the multilayer samples annealed at ≤500°C is comparable to that of some previously reported Cu interconnect structures with an Ru based barrier.[21–23] The 600°C-annealed sample has a leakage current density as high as 4.7×10^{-4} A/cm^2 at

Downloaded on 2014-04-24 to IP 140.113.38.11 address. Redistribution subject to ECS terms of use (see ecsdl.org/site/terms_use) unless CC License in place (see abstract).

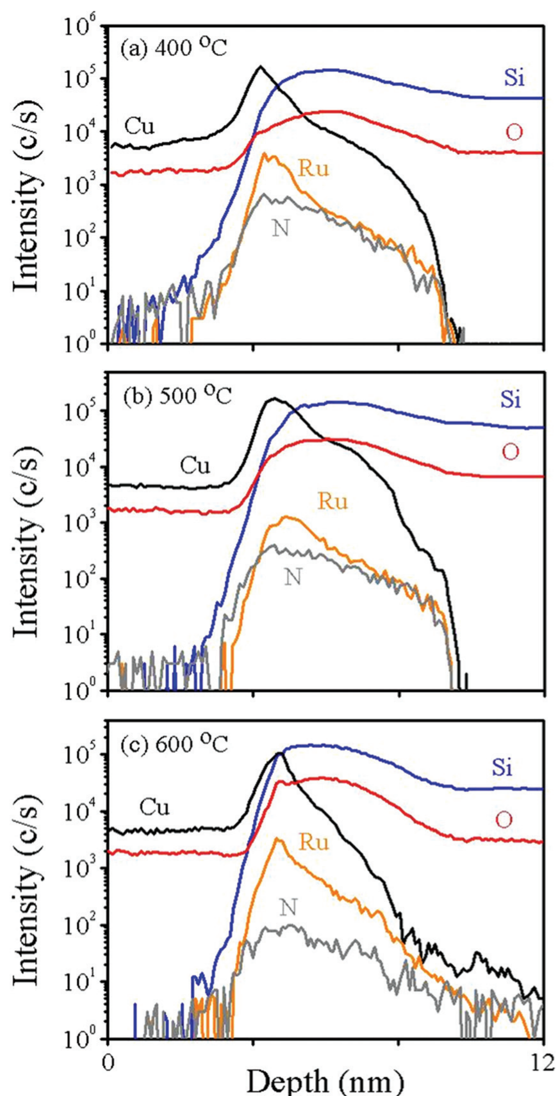

Figure 8. (Color online) SIMS depth profiles of (a) the 400°C-annealed, (b) the 500°C-annealed, and (c) the 600°C-annealed Cu/Ru/RuN_x/*mp*-SiO_2 multilayer stacks. The profile data in the Cu layer are mostly truncated so that the interface region can be clearly examined.

1 MV/cm, suggesting that metallic impurities may diffuse into the dielectric layer as a result of the extensive thermal breakdown of the Ru/RuN_x bilayer.

Although the Ru/RuN_x bilayer capped with the electroplated Cu can physically and chemically withstand the thermal anneal at temperatures as high as 500°C, the material and electrical characterizations discussed above do not provide information about the mechanical strength of the multilayer stack. We thus studied the interface adhesion of the Cu/Ru/RuN_x/*mp*-silica mutilayer stack by pull-off tensile test, and the result is shown in Fig. 10. The adhesion strength of the the mutilayer is within the range between 46 and 48 kg/cm^2 for samples annealed at 400 and 500°C, while the adhesion strength of the sample annealed at 600°C drastically drops to ~2 kg/cm^2. The adhesion strength of the Cu/Ru/RuN_x/*mp*-SiO_2 sample annealed at temperatures ≤500°C is comparable to that of the Cu/TaN_x/*mp*-SiO_2 structure reported in our previous study.[24] For the 400- and 500°C-annealed samples, the mechanical failure during the pull-off test takes place at the interface between the Ru/RuN_x barrier layer and the electroplated Cu layer according to ESCA analysis. This is opposite to the 600°C-annealed sample, in which the delamination occurs at the interface between the barrier layer and the *mp*-SiO_2 layer. This adhesion test indicates the in situ two-step PEALD process can deposit an Ru/RuN_x barrier layer strongly adhering to the mesoporous dielectric layer.

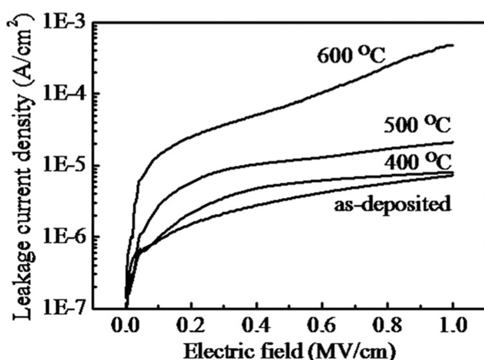

Figure 9. The leakage current density of the Cu/Ru/RuN_x/*mp*-SiO_2/Si/Al multilayer samples as a function of the annealing temperature.

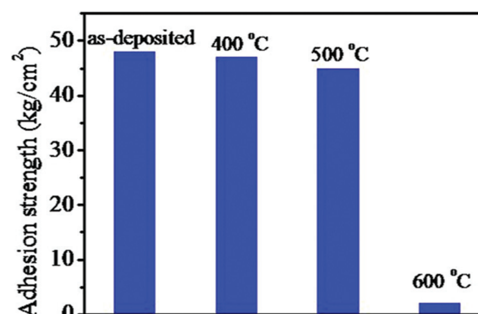

Figure 10. (Color online) Bar diagrams of the adhesion strength of the Cu/Ru/RuN_x/*mp*-SiO_2 multilayer stack as a function of the annealing temperature.

Conclusion

We prepared Ru/RuN_x diffusion barriers on mesoporous SiO_2 thin films by PEALD for the application of seedless Cu electroplating. The 4 nm thick Ru/RuN_x bilayer was deposited on the porous dielectric substrate at 200°C using the in situ two-step PEALD process. Obvious thermal degradation occurs to the bare Ru/RuN_x bilayer at temperatures ≤400°C, and direct Cu electroplating is successful only on the as-deposited bilayer barrier. The electroplated Cu layer behaves like a passivation layer that can impede thermal degradation of the Ru/RuN_x barrier. The Cu/Ru/RuN_x/*mp*-SiO_2 multilayer structure can withstand the thermal treatment without significant physical and chemical degradations at temperatures ≤500°C according to TEM and SIMS analyses. The 400- and the 500°C-annealed samples have a low leakage current density. When the Cu capped multilayer sample is annealed at 600°C, thermal decomposition of the RuN_x layer results in metal diffusion into the *mp*-SiO_2 layer and delamination at the interface between the Ru/RuN_x bilayer and the dielectric layer. The pull-off tensile test shows that, at temperatures ≤500°C, interfaces in the Cu/Ru/RuN_x/*mp*-SiO_2 multilayer stack have a good adhesion strength. The study has demonstrated that the PEALD Ru/RuN_x bilayer structure prepared using the in situ two-step approach is suitable for the seedless Cu electroplating process in nanometer scale interconnect technology.

Acknowledgments

This work was supported by the National Science Council of R.O.C. under Contract No. NSC97-2221-E-009-016-MY3. Technical supports from National Nano Device Laboratories is gratefully acknowledged.

National Chiao Tung University assisted in meeting the publication costs of this article.

Downloaded on 2014-04-24 to IP 140.113.38.11 address. Redistribution subject to ECS terms of use (see ecsdl.org/site/terms_use) unless CC License in place (see abstract).

References

1. International Technology Roadmap for Semiconductors (ITRS), 2007 edition, http://public.itrs.net/.
2. J. D. Kwon, S. J. Jeong, J. W. Kang, D. G. Kim, J. K. Kim, J. J. Rha, K. S. Nam, and S. H. Kwon, *J. Electrochem. Soc.*, **156**, H832 (2009).
3. S. Cho, K. Lee, P. Song, H. Jeon, and Y. Kim, *Jpn. J. Appl. Phys.*, **46**, 4085 (2007).
4. B. Lee, K. J. Choi, A. Hande, R. M. Wallace, J. Kim, Y. Senzaki, D. Shenai, H. Li, M. Rousseau, and J. Suydam, *Microelectron. Eng.*, **86**, 272 (2009).
5. C.-C. Yang, S. Cohen, T. Shaw, P.-C. Wang, T. Nogami, and D. Edelstein, *IEEE Electron Device Lett.*, **31**, 722 (2010).
6. T. N. Arunagiri, Y. Zhang, and O. Chyan, *Appl. Phys. Lett.*, **86**, 083104 (2005).
7. D. Josell, C. Witt, and T. P. Moffat, *Electrochem. Solid-State Lett.*, **9**, C41 (2006).
8. D. Josell, J. E. Bonevich, T. P. Moffat, T. Aaltonen, M. Ritala, and M. Leskela, *Electrochem. Solid-State Lett.*, **9**, C48 (2006).
9. *Binary Alloy Phase Diagrams,* 2nd ed., T. B. Massalski, Editor, p. 1467, American Society of Metals, Materials Park (1990).
10. R. Chan, T. N. Arunagiri, Y. Zhang, O. Chyan, R. M. Wallace, M. J. Kim, and T. Q. Hurdc, *Electrochem. Solid-State Lett.*, **7**, G154 (2004).
11. M. Damayanti, T. Sritharan, S. G. Mhaisalkar, and Z. H. Gan, *Appl. Phys. Lett.*, **88**, 044101 (2006).
12. M. Damayanti, T. Sritharan, S. G. Mhaisalkar, H. J. Engelmann, E. Zschech, A. V. Vairagar, and L. Chan, *Electrochem. Solid-State Lett.*, **10**, P15 (2007).
13. N. Torazawa, T. Hinomura, K. Mori, Y. Koyama, S. Hirao, E. Kobori, H. Korogi, K. Maekawa, K. Tomita, H. Chibahara, et al., in *Proceedings of IEEE International Interconnect Technology Conference (IITC)*, p. 113 (2009).
14. J. P. Chu and C. H. Lin, in *Proceedings of IEEE International Interconnect Technology Conference (IITC)*, p. 25 (2008).
15. C. M. Yang, A. T. Cho, F. M. Pan, T. G. Tsai, and K. J. Chao, *Adv. Mater.*, **13**, 1099 (2001).
16. C. C. Chang, F. M. Pan, and C. W. Chen, *Microelectron. Eng.*, **86**, 2241 (2009).
17. O. K. Kwon, S. H. Kwon, H. S. Park, and S. W. Kang, *J. Electrochem. Soc.*, **151**, C753 (2004).
18. Joint Committee for Powder Diffraction Standards (JCPDS) Card No. 06-0663.
19. C. Ryu, K. W. Kwon, A. L. S. Loke, H. Lee, T. Nogami, V. M. Dubin, R. A. Kavari, G. W. Ray, S. S. Wong, *IEEE Trans. Electron Devices*, **46**, 1113 (1999).
20. R. G. Wilson, F. A. Stevie, and C. W. Magee, *Secondary Ion Mass Spectrometry*, John Wiley & Sons, New York (1989).
21. J. B. Yeh, D. C. Perng, and K. C. Hsu, *J. Electrochem. Soc.*, **157**, H810 (2010).
22. D. C. Perng, K. C. Hsu, S. W. Tsai, and J. B. Yeh, *Microelectron. Eng.*, **87**, 365 (2010).
23. D. C. Perng, J. B. Yeh, and K. C. Hsu, *Appl. Surf. Sci.*, **256**, 688 (2009).
24. C. C. Chang, F. M. Pan, and C. W. Chen, *J. Electrochem. Soc.*, **157**, G62 (2010).

Downloaded on 2014-04-24 to IP **140.113.38.11** address. Redistribution subject to ECS terms of use (see **ecsdl.org/site/terms_use**) unless CC License in place (see abstract).